cells

MDPI

Article

Machine learning allows distinguishing precancerous and cancerous human epithelial cervical cells using high-resolution AFM imaging of adhesion maps

M. Petrov [1] and I. Sokolov [1,2,*]

[1] Department of Mechanical Engineering, Tufts University, Medford, MA 02155, USA;
[2] Departments of Physics and Biomedical Engineering, Tufts University, Medford, MA 02155, USA
* Correspondence: igor.sokolov@tufts.edu*

Abstract: Previously, the analysis of atomic force microscopy (AFM) images allowed us to distinguish normal from cancerous/precancerous human epithelial cervical cells using only the fractal dimension parameter. High-resolution maps of adhesion between the AFM probe and the cell surface were used in that study. However, the separation of cancerous and precancerous cells was rather poor (the area under the curve (AUC) was only 0.79, whereas the accuracy, sensitivity, and specificity were 74%, 58%, 84%, respectively). At the same time, the separation between premalignant and malignant cells is the most significant from a clinical point of view. Here, we show that the introduction of machine learning analysis of the adhesion maps allows distinguishing precancerous and cancerous cervical cells with a rather good precision (AUC, accuracy, sensitivity, and specificity are 0.93, 83%, 92%, 78%, respectively). Substantial improvement in sensitivity is significant because of the unmet need in clinical practice to improve the screening of cervical cancer (a relatively low specificity can be compensated by combining this approach with other currently existing screening methods). The Random Forest decision tree algorithm was utilized in this study. The analysis was done using the data of six precancerous primary cell lines and six cancerous primary cell lines, each derived from different humans. The robustness of the classification was verified by K-fold cross-validation (K=500). The results are statistically significant at $p< 0.0001$. Statistical significance was determined using the random shuffle method as a control.

Keywords: cancer detection; machine learning; atomic force microscopy (AFM); scanning probe microscopy (SPM)

Citation: To be added by editorial staff during production.

Academic Editor: Firstname Lastname

Received: date
Revised: date
Accepted: date
Published: date

1. Introduction

Morbidity and mortality associated with cervical cancer are substantially decreased when cancer is detected early [1-3]. Thus, the search for new approaches to early diagnosis is of great significance. Cervical cancer is the second most frequent type of cancer among women worldwide with approximately 288,000 deaths per year; more than 14,000 women were diagnosed with this disease in 2022 in the US along [4-6]. The mortality rate is second only to that for breast cancer. Early detection of cervical cancer using the Papanicolaou (Pap) smear test has decreased mortality from cervical cancer by 70 - 80% [5,7]. Early detection is based on the identification of neoplastic cells in stained preparations obtained from the uterine cervix [7].

It should be noted that recently introduced DNA-HPV tests are broadly used these days. It is a good screening test because approximately 95% of cases of this cancer correlate with the presence of human papillomavirus (HPV). However, the accuracy of cancer detection (sensitivity) of DNA-HPV tests is low. For example, only 43% of HPV-positive females diagnosed in Massachusetts (USA) from 2004 to 2014 had cervical cancer [8].

Recent studies have shown that DNA-HPV tests are particularly ineffective among young women who have this virus much more frequently than cervical cancer. Thus, the interest in Pap smear tests is growing again.

The main advantages of Pap smear cytological test are their simplicity and minimal invasiveness (the cells are obtained from the cervix using a combination of a spatula and brush). Despite the impressive success of these tests, their sensitivity for detecting preinvasive cervical lesions is far from desirable, with a mean sensitivity of only 47% (range 30 - 80%). The sensitivity of the cytological tests for invasive carcinoma (cancer cells) is not perfect, ranging from 16% to 82% in different studies [5,9]. According to the American Cancer Society data, each year in the United States alone, approximately 3.6 million cytological tests are classified as equivocal, out of which only 8% of women will have preinvasive (high-grade squamous intraepithelial) lesions, and 0.4% will have carcinoma as found in further testing that involves invasive tissue biopsies. This means that more than 3.3 million biopsies per year may be unnecessary if a more accurate screening of cervical cancer is invented. In addition to the relatively low sensitivity of the cytological tests and moderate reproducibility of the diagnosis, there are sampling and laboratory errors. Finally, there are inherent problems of the identification of malignant cells with cytological test methodology. More accurate tests may substantially decrease the cost and patient inconvenience of screening by eliminating additional steps of colposcopy [10] . However, further improvement of cytological tests may have fundamental restrictions inherent to the limitations of morphologic analysis by means of optical microscopy.

Here we used a method of analysis of the cervical epithelial cells by means of atomic force microscopy (AFM). This microscopy has a substantial resolution advantage (200-5000 times) compared with optical microscopy. It is superior to even electron microscopy when applied to soft materials. There have been multiple partially successful attempts to use surface analysis of cell images to identify cancer cells [11,12]. The AFM technique has been previously used to study cells [13-16] [17,18], including cancerous cervical cells [19,20]. Recently introduced AFM modalities such as Peak Force QNM, HarmoniX, Ringing mode, etc. allow obtaining different properties physical properties of the cell surface, which is impossible to obtain with any other microscopy.

Previously, we have demonstrated the analysis of the AFM collected maps of adhesion between the AFM probe and the surface of human cervical epithelial cells [21,22]. The cells needed for this approach can be collected using methods similar to Pap smear cytological tests [22,23]. Essentially, the difference is in the use of different fixative, temperature, and time of fixation. The analysis has shown that it is possible to unambiguously distinguish normal from cancerous/precancerous cells by just using one parameter of the fractal dimension of the adhesion maps. Being definitely innovative, the practical utility of such a finding was limited because the separation between precancerous and cancerous cells was rather poor. Specifically, the area under the curve (AUC) was only 0.79, whereas the accuracy, sensitivity, and specificity were 0.74, 0.58, 0.84, respectively. From the clinical utility point of view, the separation between premalignant and malignant cells would be the most significant because it leads to the improvement of the existing Pap smear tests. It is rather difficult to distinguish between such cells using just optical microscopy.

Here, we show that the introduction of machine learning analysis of the adhesion maps leads to a substantial improvement in the detection of cancer cells with respect to the previous results based on just fractal dimension. The values of AUC, accuracy, sensitivity, and specificity are 0.93, 83%, 92%, 78%, respectively). It has to be stressed that the fund increase in sensitivity while keeping the number of missed cancerous low is the currently existing unmet need in clinical practice. With the sensitivity of 92%, the percentage of missed cancer cases (false negative rate) is only 7%, which much better than better

than the modern invasive colposcopy tests [24]. The analysis is applied to the adhesion maps collected on six primary precancerous and six primary cancerous cell lines; each cell line is extracted from a different patient.

2. Results and Discussion

As has been found in the previous study [21,22], 10x10 μm² is the most effective AFM scan size to discriminate between normal and cancerous cells. Figure 1 shows examples of typical height and adhesion images of this size for cancerous and precancerous cells. The main conclusion from these images is the difficulty of discriminating between these cell phenotypes by just visual judgment. To discriminate between normal and cancerous cells in a quantitative way, it was suggested to look at the characteristics of fractal geometry of the cell surface and their adhesion maps [21,22]. The same study showed that the height images provide very little discriminating power compared to the adhesion maps. Following this conclusion, we will not use the height images to analyze the differences between cancerous and precancerous cells and focus on the adhesion images.

The most popular image recognition these days is deep learning, specifically convolution neural networks (CNN), see, e.g., [25]. However, this analysis works well if there is a sufficient number of images available for training. The AFM technique, being a relatively slow microscopy, does not allow the generation of a very large number of images. It creates a number of challenges in building CNN algorithms when applied to the classification of cells [26]. Furthermore, neural networks are particularly prone to overtraining. As a result, we suggest using other machine learning algorithms, like decision trees. Specifically, we used a bootstrap of decision trees called Random Forest [27,28]. The important part of our approach is the reduction of data space. Instead of analyzing 512 x 512 pixels to characterize each AFM scan, we converted each scan into a set of "surface parameters", see the Method section for detail. Such parameters are used in engineering to describe quality of surfaces [29]. We chose five surface parameters in addition to the fractal dimension parameter introduced in [21,22]. These parameters were chosen because they demonstrated the biggest difference in their average values between cancer and normal cells. These parameters (see, their description in detail in the methods section) represent various characteristics of the surface roughness.

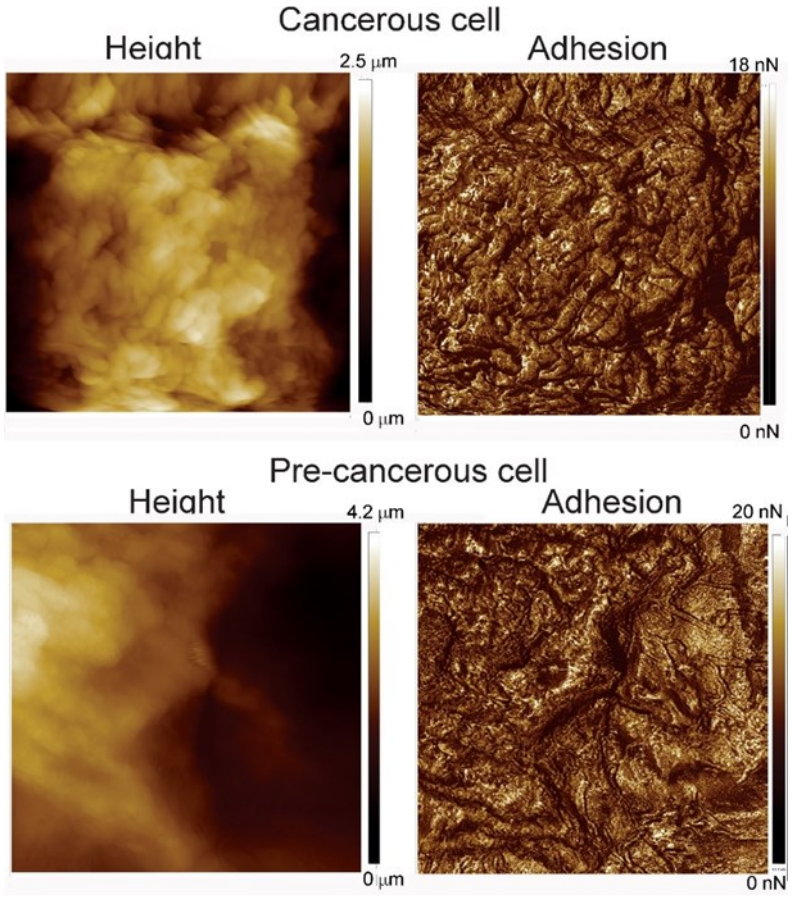

Figure 1. Examples of typical 10x10 μm² AFM images of precancerous and cancerous cells used in the study.

Figure 2 demonstrates the entire process of data analysis. All AFM images of the adhesion are converted into a set of the chosen six surface parameters. Then, the obtained database is randomly split into the training and testing subsets. The split was chosen to be 70 and 80% for the training and 30 and 20% for the testing subsets, respectively. The final result is the same for these two particular particular splits. After creating the machine learning algorithm by training Random Forest on the training subset, the statistical analysis of the obtained algorithm was done on the testing subset. The statistical analysis includes the ROC (receiver operating characteristic) curve and the confusion matrix. ROC curve allows to define a range of sensitivity ("accuracy" of identification of cancer cells) and specificity ("accuracy" of identification of absence of cancer cells), and the accuracy. These quantities are defined as follows: sensitivity = TP/(TP+FN); specificity = TN/(TN+FP); accuracy= (TN+TP)/(TP+FN+TN+FP), where TP, TN FP, FN are the true positive, true negative, false positive, and false negative components of the confusion matrix.

Because the machine learning algorithms are too complicated to be easily verified, it is important to test the robustness of the obtained results. It is done by using the K-fold cross-validation and verification of the absence of overtraining. To do the K-fold cross-validation, we repeated the random split between testing and training databases 500 times (we also observed that a further increase of the number of these splits to 1000x does not change the obtained statistics). This way, we can calculate not only the average values of the ROC curve and the components of the confusion matrix but also their standard deviations. Technically, this approach verifies the absence of overtraining because the calculated statistics are done on the testing subsets that are completely separated from and independent of the training ones. For example, if the distribution of AUC is rather

narrow (small standard deviation compared to the average), the algorithmic approach has no overtraining.

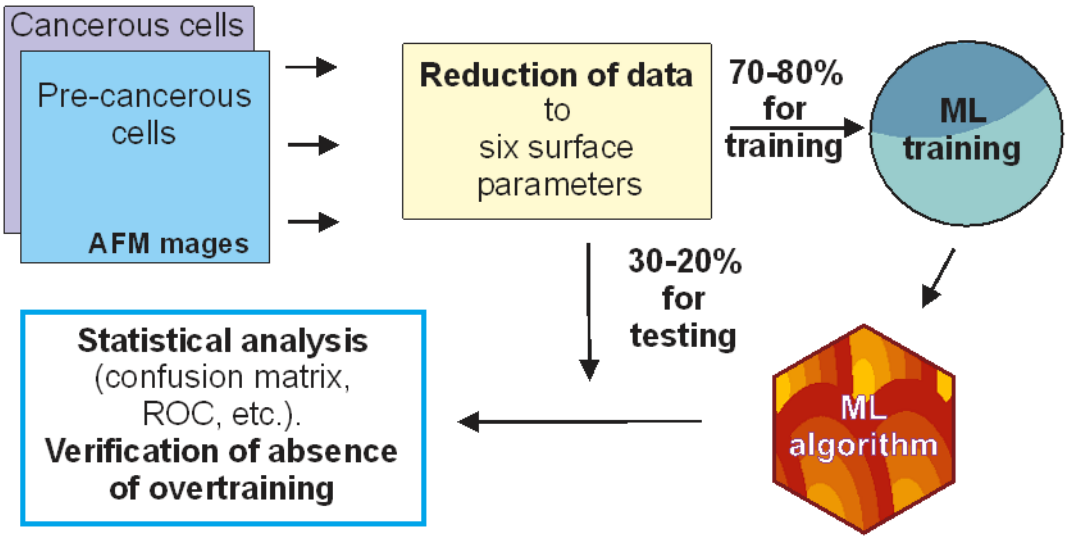

Figure 2. Schematics of machine learning (ML) analysis. Conversion of the AFM images into the surface parameters; splitting the database into the training and testing subsets; developing an ML algorithm using just the training subset; using the testing subset to do the statistical analysis of the developed ML algorithm; and finally, cross-validation and verification of the lack of overtraining of the developed approach.

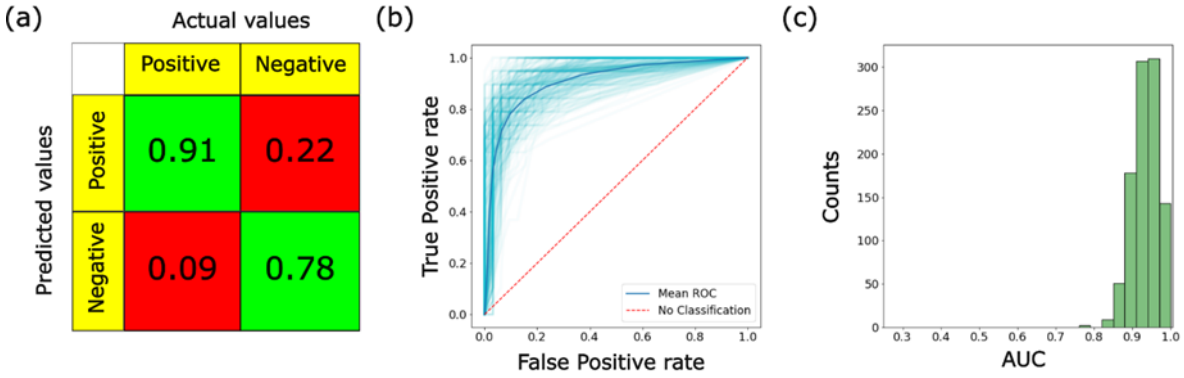

Figure 3. Results of the ML analysis of the difference between precancerous and cancerous cells. (a) Confusion matrix, (b) ROC curves, and (c) histogram of the areas under the curve (AUC).

Figure 3 shows the result of the described analysis. The confusion matrix demonstrates the average values of TP, TN FP, FN equal to 0.91, 0.78, 0.22, and 0.09, respectively. AUC, accuracy, sensitivity, and specificity are 0.93, 83%, 92%, 78%, respectively. This is a substantial improvement compared to the previously reported values of 0.79, 74%, 58%, 84%, respectively. It is important to note that at first glance, the improvement might not look that substantial because of a slight decrease in the specificity. However, it is the increase in sensitivity that is urgently needed in clinical practice. As we described in the Introduction, the existing screening tests for cervical cancer (Pap smear) are effective (decreased mortality from cervical cancer by 70 -80%) but insufficiently accurate (mean sensitivity of only 47% (range 30 - 80%)). It leads to a high number of unnecessary invasive biopsy (colposcopy). The other broadly used screening HPV tests demonstrate 95-100% specificity, however, low in sensitivity (HPV tests do not detect cancer but just identify people at high risk of getting this cancer). As was mentioned, only 43% of HPV-associated cancers diagnosed in Massachusetts females from 2004-2014 had cervical cancer. As a result of the low sensitivity of the existing non-invasive tests, millions of invasive and

expensive biopsies (colposcopies) are done each year. If there were a noninvasive screening test with 95% sensitivity, 3.1 million biopsies per year in the US (based on 2022 data) could be unnecessary. Therefore, the fact that we observed a substantial improvement in sensitivity (58% -> 92%) is very promising.

It also should be noted that the most accurate measure of the improvement of the method is the value of AUC. The other statistical parameters discussed here depend on a particular threshold of probability of the classifier, which defines which class each tested cell belongs. Moving this threshold, one can, for example, increase sensitivity at the expense of specificity. To avoid this ambiguity, one should remember the final goal of the described method, the detection of the presence of cancer cells. Secondly, the method should miss the cancer cases to the maximum possible extent. The latter is described by the false negative rate, which is calculated as FN/(FN+TP). For the calculations presented in this work, the false negative rate is within 7%. This is substantially better than the modern invasive colposcopy tests [24]. It can be improved even further by combining several cells for the diagnosis. Nevertheless, it should be remembered that the present results are done on cell lines. So, it is a proof of the concept. To claim the development of a new clinical method, the present method has to be applied to cells obtained from actual patients.

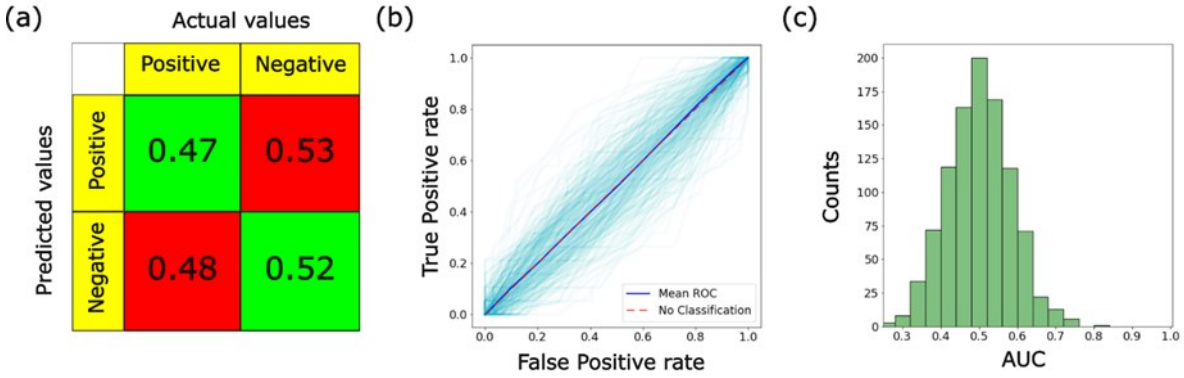

Figure 4. Further verification of the lack of overtraining of the ML algorithm used in this work: shuffled class assignment of the data (a) Confusion matrix, (b) ROC curves, (c) histogram of the areas under the curve (AUC). These AUC data are also used to find the statistical significance of the results shown in Fig.3.

Although the Random Forest method is known not to have serious problems with overtraining, it is instructional to further verify the absence of overtraining. To do that, we use the method suggested in [30]. Furthermore, this method will allow us to find the statistical significance of the obtained results. In this method, it was suggested that a correct non-overtrained algorithm should give the correct AUC of 0.5 (no-classification value) for a completely randomized test set. The same should be seen for the confusion matrix. To exclude a coincidental choice of the correct class assignment, the process of randomization was repeated 500 times as well (the same idea as in the K-fold cross-validation). Figure 4 demonstrates the results of such calculations. The area under ROC curve is indeed equal to 0.5 with rather high precision. The average accuracy is also around 50%.

The described above data obtained on the completely randomized test sets can also be used to find the statistical significance of the results of this work. To do that, we suggest using the AUC data obtained on the actual training data set and the AUC data obtained using the same algorithm but applied to the complete randomized test sets. Since the method correctly identified the absence of any signal (randomness of the class association), it can be considered as a control data set. Using ANOVA one-side statistical test and

the data generated for 500-fold cross-validation, we found that the obtained results are statistically significant at the confidence level $p < 0.0001$.

Let us now discuss the nature of the observed differences between precancerous and cancerous cells. The difference in the pericellular layer of cancerous and normal cells has been reported in the literature [31] using atomic force microscopy, in particular, the modality capable of imaging the distribution of the adhesion. This is novel because it gives unique information about the cell surface, which includes not only the surface morphology of cells but also the maps of the adhesive properties of cells. And because it is novel, there are no biochemical information available that connects such properties with known biochemical pathways. The previously observed difference in the cell microvilli of cancerous cells [20] is unlikely to be the only reason responsible for the observed difference because such structures are detectable by electronic and even optical microscopy, which has been broadly used in multiple reports in which no substantial difference between normal or cancer cells was found. In addition, the topographical AFM images of the cell surface, in which the microvilli and microridges are perfectly seen, did not show a statistically significant difference between cancer and normal cells [21,22].

The complexity of the challenge to link the observed data to the biochemical processes inside the cell was demonstrated in ref. [22] by the analysis of fractal dimensions, in particular, the concept of multi-practicality. Fractals are complex disorderly patterns that typically occur under far-from-equilibrium conditions [32] and/or emerge from chaos [33]. Fractal shapes are found in the large-scale structure of the Universe [34], continental coastlines [35], trees [36], grain structures of materials[37], clouds [38], and even artistic creations [39]. There are many models describing the emergence of fractal geometry [33,40]. However, neither of the models explains the emergence of fractal geometry on cells. Therefore, we expect it to be a challenge for the future. As of now, it can be used for practical medical applications like the detection of cancer, specifically, in combination with the existing screening HPV and Pap smear tests.

3. Methods

Cells and AFM imaging

The cell lines, AFM imaging, and sample preparation were descired in our previous works [21,22]. Here we just briefly describe it. Twelve different human cervical epithelial cell lines were prepared from tissues collected from the transformation zone of the cervix from six cancer and six healthy patients. The human tissues were received from the Cooperative Human Tissue Network. Cells were extracted by a two-stage enzymatic digestion with dispase enzyme to remove the epithelium and then trypsin to disperse the individual epithelial cells [41]. To prepare precancerous (immortal) cells, normal cells (extracted from healthy individuals) were transfected and then immortalized using HPV-16 virus. After a number of passages, all non-immortilized cells died out after 60–150 population doublings**.** All cells were used for experiments when cells were subconfluent (<50% confluency). Created this way precancerous CX-16–2, 16–4, 16–11, 16–12, 16–14, 16–15, and cancerous CXT-2, 3, 5, 6,7,8 cell lines were used for the AFM imaging. In total, images of 64 cancerous cells and 108 precancerous cells were used in this study. The data used in this work can be downloaded from the online database [42].

For the AMF study, cells were fixed with Karnovsky's fixative as described in [21,22]. In brief, cells cultured in 60 mm Petri dishes were washed twice with PBS buffer, and then treated with 4ml of Karnovsky's fixative overnight at 4°C. Fixed cells were flushed from Karnovsky's fixative with 5 ml of DI water twice (one time for several hours). For imaging, cells were dried using a freeze dryer and stored in a desiccator. As we showed in ref. [22], cells should be imaged under humidity not exceeding 60-65%. The actual imaging was done under the relative humidity not exceeding 50%. A Nanoscope™ Dimension

3100 AFM (Veeco/Bruker-Nano, Inc., Santa Barbara, CA) with Nanoscope V controller working in HarmoniX mode was employed. A standard cantilever holder with HarmoniX standard cantilevers for operation in air were used.

Surface parameters used in the study

The surface parameters used in this work include Surfaces Area Ratio (*Sdr*), Root Mean Square Gradient (*Sdq*), Reduced Summit Height (*Spk*), and the fractal dimension. On the top of it, we also used two fractal dimensions introduced in our previous work [21,22], *Sfd_top*, and *Sfd_bottom*, which are the fractal dimensions calculated for the surface features above and below 300 nm in size, respectively. Below, we give the formulas for the calculation of the used surface parameters.

The Surfaces Area Ratio (Sdr) represents the increase of the interfacial surface area relative to the area of the projected (flat) *x*, *y* plane:

$$S_{sdr} = \frac{\left(\sum_{k=0}^{M-2}\sum_{l=0}^{N-2} A_{kl}\right) - (M-1)(N-1)\delta x \delta y}{(M-1)(N-1)\delta x \delta y} 100\%,$$

where A_{kl} is defined as:

$$A_{kl} = \frac{1}{4}\left(\sqrt{\delta y^2 + \left(z(x_k, y_l) - z(x_k, y_{l+1})\right)^2} + \sqrt{\delta y^2 + \left(z(x_{k+1}, y_l) - z(x_{k+1}, y_{l+1})\right)^2}\right) \cdot \left(\sqrt{\delta y^2 + \left(z(x_k, y_l) - z(x_{k+1}, y_l)\right)^2} + \sqrt{\delta y^2 + \left(z(x_k, y_{l+1}) - z(x_{k+1}, y_{l+1})\right)^2}\right)$$

The Root Mean Square Gradient (Sdq) is the RMS-value of the surface slope within the sampling area. It is defined as:

$$S_{dq} = \sqrt{\frac{1}{(M-1)(N-1)}\sum_{k=0}^{M-1}\sum_{l=0}^{N-1}\left(\frac{z(x_k, y_l) - z(x_{k-1}, y_l)}{\delta x}\right)^2 + \left(\frac{z(x_k, y_l) - z(x_k, y_{l-1})}{\delta y}\right)^2}$$

.

Reduced Summit Height (Spk). This parameter is calculated using an algorithm in an implicit way. It is calculated based on the bearing area ratio curve. To find it, one needs to draw a line fitted to the 40% segment of the curve that results in the lowest decline (using the least mean squares). Man, this line is extrapolated until it crosses the vertical axes of the bearing area ratio curve for 0% and 100%. Then, two horizontal lines are drawn through the intersection points. Finally, a straight line that starts at the intersection point between the bearing area ratio curve and the upper horizontal line and ends on the 0% axis should be drawn in a way that the area of the obtained triangle is the same as the area between the horizontal line and the bearing area ratio curve. Using the same algorithm, a line between the lower horizontal line and the 100% axis should be drawn. The Reduced Summit Height (*Spk*) is the value of the height of the upper left triangle.

Fractal dimensions. Calculation of the fractal dimensions was done with the help of SPIP software following the method described in [40]. The method is based on the use of two-dimensional Fourier transformation:

$$F(u,v) = \frac{1}{N_x N_y}\sum_{x=0}^{N_x-1}\sum_{y=0}^{N_y-1} z(x,y) e^{-i2\pi(ux/N_x + vy/N_y)},$$

where N_x, N_y are the number of pixels in the *x*, *y* directions and *u*, *v* the discrete Fourier indexes =0, 1, 2, ... N_{x-1} and *v* = 0, 1, 2 ... N_{y-1}.

The obtained career spectrum was averaged over all possible directions to convert this spectrum into 1D. The resulting spectrum is only a function $A(Q)$ of reciprocal space coordinate Q or the inverse lateral size of the geometrical features on the AFM image. The fractal dimension was calculated using the expected power-law behavior $A(Q) \sim Q^b$. Specifically, the fractal dimension was defined as $2-b$. Two fractal dimensions were calculated, below (*Sfd_top*) and above (*Sfd_bottom*) $Q=1/300\ nm^{-1}$. Both fractal dimensions were used in the machine learning analysis described in this work as two separate parameters.

It has to be noted that ideologically, the use of the surface parameters to analyze the maps of adhesion is a substantial departure from the classically considered surface parameters. When we use the previously suggested formulas, they contain a mix of quantities of different dimensions. Although it does not imply any specific restrictions when these parameters are used in machine learning, obviously, the answer should depend on which particular units we use. For example, many parameters will be different if we use the presentation of adhesion force in N (Newtons), μN, or nN. Therefore, the choice of particular units has to be consistent along all measurements. Specifically, here, we found that the largest difference between cancerous and precancerous cells was observed when the adhesion force is used in nanoNewtons, and the spatial dimensions are in the nanometers.

Acknowledgments Support of this work by NIH R01 CA262147, the MLSC Bit-to-Bites program, and the NSF CMMI 2224708 grants is acknowledged.

Author Contributions I.S. conceived and designed the experiments and data analysis and did a part of the statistical analysis; M.P. did the data analysis.

References

1. Costa, S.; Negri, G.; Sideri, M.; Santini, D.; Martinelli, G.; Venturoli, S.; Pelusi, C.; Syrjanen, S.; Syrjanen, K.; Pelusi, G. Human papillomavirus (HPV) test and PAP smear as predictors of outcome in conservatively treated adenocarcinoma in situ (AIS) of the uterine cervix. *Gynecol Oncol* **2007**, *106*, 170-176, doi:S0090-8258(07)00213-2 [pii]10.1016/j.ygyno.2007.03.016.
2. Hanley, K.Z.; Tadros, T.S.; Briones, A.J.; Birdsong, G.G.; Mosunjac, M.B. Hematologic malignancies of the female genital tract diagnosed on liquid-based Pap test: Cytomorphologic features and review of differential diagnoses. *Diagn Cytopathol* **2009**, *37*, 61-67, doi:10.1002/dc.20994.
3. Hoda, R.S.; Colello, C.; Roddy, M.; Houser, P.M. "Fruiting body" of Aspergillus species in a routine cervico-vaginal smear (Pap test). *Diagn Cytopathol* **2005**, *33*, 244-245, doi:10.1002/dc.20267.
4. Bryushinin, M.; Golubev, V.; Kumzerov, Y.; Kurdyukov, D.; Sokolov, I. Non-steady-state photo-EMF in nanostructured GaN and polypyrrole within porous matrices. *Appl Phys B-Lasers O* **2009**, *95*, 489-495, DOI 10.1007/s00340-009-3388-0.
5. Grubisic, G.; Klaric, P.; Jokanovic, L.; Soljacic Vranes, H.; Grbavac, I.; Bolanca, I. Diagnostic approach for precancerous and early invasive cancerous lesions of the uterine cervix. *Coll Antropol* **2009**, *33*, 1431-1436.
6. Franco, E.L.; Schlecht, N.F.; Saslow, D. The epidemiology of cervical cancer. *Cancer J* **2003**, *9*, 348-359.
7. Saslow, D.; Runowicz, C.D.; Solomon, D.; Moscicki, A.B.; Smith, R.A.; Eyre, H.J.; Cohen, C.; American Cancer, S. American Cancer Society guideline for the early detection of cervical neoplasia and cancer. *CA Cancer J Clin* **2002**, *52*, 342-362.
8. The information can be found at https://www.mass.gov/doc/cervical-cancer-in-massachusetts-2004-2014/download
9. Saslow, D.; Runowicz, C.D.; Solomon, D.; Moscicki, A.B.; Smith, R.A.; Eyre, H.J.; Cohen, C. American Cancer Society guideline for the early detection of cervical neoplasia and cancer. *CA Cancer J Clin* **2002**, *52*, 342-362.
10. Katki, H.A.; Wentzensen, N. How might HPV testing be integrated into cervical screening? *Lancet Oncol* **2012**, *13*, 8-10.
11. Doornewaard, H.; van der Schouw, Y.T.; van der Graaf, Y.; Bos, A.B.; van den Tweel, J.G. Observer variation in cytologic grading for cervical dysplasia of Papanicolaou smears with the PAPNET testing system. *Cancer* **1999**, *87*, 178-183.
12. Losa, G.A. Fractals in pathology: are they really useful? *Pathologica* **1995**, *87*, 310-317.
13. Pelling, A.E.; Li, Y.; Shi, W.; Gimzewski, J.K. Nanoscale visualization and characterization of Myxococcus xanthus cells with atomic force microscopy. *Proc Natl Acad Sci U S A* **2005**, *102*, 6484-6489, doi:0501207102 [pii]10.1073/pnas.0501207102.
14. Matzke, R.; Jacobson, K.; Radmacher, M. Direct, high-resolution measurement of furrow stiffening during division of adherent cells. *Nat Cell Biol* **2001**, *3*, 607-610.
15. Suresh, S. Biomechanics and biophysics of cancer cells. *Acta Biomater* **2007**, *3*, 413-438, doi:S1742-7061(07)00061-X [pii]10.1016/j.actbio.2007.04.002.
16. Sokolov, I. Atomic Force Microscopy in Cancer Cell Research. In *Cancer Nanotechnology – Nanomaterials for Cancer Diagnosis and Therapy*, Webster, H.S.N.a.T., Ed.; APS: Los Angeles, 2007; pp. 43-59.

17. Lekka, M.; Laidler, P.; Ignacak, J.; Labedz, M.; Lekki, J.; Struszczyk, H.; Stachura, Z.; Hrynkiewicz, A.Z. The effect of chitosan on stiffness and glycolytic activity of human bladder cells. *Biochim Biophys Acta* **2001**, *1540*, 127-136.
18. Sokolov, I.; Iyer, S.; Subba-Rao, V.; Gaikwad, R.M.; Woodworth, C.D. Detection of surface brush on biological cells in vitro with atomic force microscopy. *Applied Physics Letters* **2007**, *91*, 023902-023901-023903.
19. Iyer, S.; Woodworth, C.D.; Gaikwad, R.M.; Kievsky, Y.Y.; Sokolov, I. Towards nonspecific detection of malignant cervical cells with fluorescent silica beads. *Small* **2009**, *5*, 2277 - 2284.
20. Iyer, S.; Gaikwad, R.M.; Subba-Rao, V.; Woodworth, C.D.; Sokolov, I. AFM Detects Differences in the Surface Brush on Normal and Cancerous Cervical Cells. *Nature Nanotechnology* **2009**, *4*, 389-393.
21. Dokukin, M.E.; Guz, N.V.; Woodworth, C.D.; Sokolov, I. Emergence of fractal geometry on the surface of human cervical epithelial cells during progression towards cancer. *New J Phys* **2015**, *17*, 033019, doi:Artn 03301910.1088/1367-2630/17/3/033019.
22. Dokukin, M.E.; Guz, N.V.; Gaikwad, R.M.; Woodworth, C.D.; Sokolov, I. Cell Surface as a Fractal: Normal and Cancerous Cervical Cells Demonstrate Different Fractal Behavior of Surface Adhesion Maps at the Nanoscale. *Physical Review Letters* **2011**, *107*, 028101, doi:ARTN 02810110.1103/PhysRevLett.107.028101.
23. Iyer, K.S.; Gaikwad, R.M.; Woodworth, C.D.; Volkov, D.O.; Sokolov, I. Physical Labeling of Papillomavirus-Infected, Immortal, and Cancerous Cervical Epithelial Cells Reveal Surface Changes at Immortal Stage. *Cell Biochemistry and Biophysics* **2012**, *63*, 109-116, doi:10.1007/s12013-012-9345-2.
24. Origoni, M.; Cantatore, F.; Sopracordevole, F.; Clemente, N.; Spinillo, A.; Gardella, B.; De Vincenzo, R.; Ricci, C.; Landoni, F.; Di Meo, M.L.; et al. Colposcopy Accuracy and Diagnostic Performance: A Quality Control and Quality Assurance Survey in Italian Tertiary-Level Teaching and Academic Institutions-The Italian Society of Colposcopy and Cervico-Vaginal Pathology (SICPCV). *Diagnostics (Basel)* **2023**, *13*, doi:10.3390/diagnostics13111906.
25. Zhou, B.; Khosla, A.; Lapedriza, A.; Oliva, A.; Torralba, A. Learning Deep Features for Discriminative Localization. *Proc Cvpr Ieee* **2016**, 2921-2929, doi:10.1109/Cvpr.2016.319.
26. Azuri, I.; Rosenhek-Goldian, I.; Regev-Rudzki, N.; Fantner, G.; Cohen, S.R. The role of convolutional neural networks in scanning probe microscopy: a review. *Beilstein J Nanotechnol* **2021**, *12*, 878-901, doi:10.3762/bjnano.12.66.
27. Khabsa, M.; Elmagarmid, A.; Ilyas, I.; Hammady, H.; Ouzzani, M. Learning to identify relevant studies for systematic reviews using random forest and external information. *Mach Learn* **2016**, *102*, 465-482, doi:10.1007/s10994-015-5535-7.
28. Breiman, L. Random forests. *Mach Learn* **2001**, *45*, 5-32, Doi 10.1023/A:1010933404324.
29. The complete list of these parameters is described in standards ISO 4287/1 ASME B46.1; ISO/DIS 25178-2 used to characterize surfaces.
30. Sokolov, I.; Dokukin, M.E.; Kalaparthi, V.; Miljkovic, M.; Wang, A.; Seigne, J.D.; Grivas, P.; Demidenko, E. Noninvasive diagnostic imaging using machine-learning analysis of nanoresolution images of cell surfaces: Detection of bladder cancer. *Proceedings of the National Academy of Sciences of the United States of America* **2018**, *115*, 12920-12925, doi:10.1073/pnas.1816459115.
31. Iyer, S.; Gaikwad, R.M.; Subba-Rao, V.; Woodworth, C.D.; Sokolov, I. Atomic force microscopy detects differences in the surface brush of normal and cancerous cells. *Nature Nanotechnology* **2009**, *4*, 389-393, doi:10.1038/Nnano.2009.77.
32. Meakin, P. *Fractals, scaling, and growth far from equilibrium*; Cambridge University Press: Cambridge, U.K. ; New York, 1998; pp. xiv, 674 p.
33. McCauley, J.L. *Chaos, dynamics, and fractals : an algorithmic approach to deterministic chaos*; Cambridge University Press: Cambridge ; New York, NY, 1993; pp. xxi, 323 p.
34. Wu, K.K.S.; Lahav, O.; Rees, M.J. The large-scale smoothness of the Universe. *Nature* **1999**, *397*, 225-230.
35. Burrough, P.A. Fractal dimensions of landscapes and other environmental data. *Nature* **1981**, *294*, 240-242.
36. Morse, D.R.; Lawton, J.H.; Dodson, M.M.; Williamson, M.H. Fractal dimension of vegetation and the distribution of arthropod body lengths. *Nature* **1985**, *314*, 731-733.
37. Chopard, B.; Herrmann, H.J.; Vicsek, T. Structure and growth mechanism of mineral dendrites. *Nature* **1991**, *353*, 409-412.
38. Lovejoy, S. Area-Perimeter Relation for Rain and Cloud Areas. *Science* **1982**, *216*, 185-187, doi:216/4542/185 [pii]10.1126/science.216.4542.185.
39. Jones-Smith, K.; Mathur, H. Fractal Analysis: revisiting Pollock's drip paintings. *Nature* **2006**, *444*, E9-10; discussion E10-11, doi:nature05398 [pii]10.1038/nature05398.
40. Falconer, K.J. *Fractal geometry : mathematical foundations and applications*; Wiley: Chichester ; New York, 1990; pp. xxii, 288 p.
41. Woodworth, C.D.; Bowden, P.E.; Doniger, J.; Pirisi, L.; Barnes, W.; Lancaster, W.D.; DiPaolo, J.A. Characterization of normal human exocervical epithelial cells immortalized in vitro by papillomavirus types 16 and 18 DNA. *Cancer research* **1988**, *48*, 4620-4628.
42. https://figshare.com/articles/dataset/Data_for_the_surface_parameters_for_paper_M_E_Dokukin_i_et_al_i_2015_i_New_J_Phys_i_b_17_b_033019_b_DOI_b_10_1088_1367-2630_17_3_033019/23810616